Orbit Determination Accuracy Analysis of the Magnetospheric Multiscale Mission During Perigee Raise

Daniel A. Pachura[1], Matthew A. Vavrina[2]
a.i. solutions, Inc., Lanham, MD 20706

and

J. Russell Carpenter[3], Cinnamon A. Wright[4]
NASA Goddard Space Flight Center, Greenbelt, MD 20771

The Goddard Space Flight Center (GSFC) Flight Dynamics Facility (FDF) will provide orbit determination and prediction support for the Magnetospheric Multiscale (MMS) mission during the mission's commissioning period. The spacecraft will launch into a highly elliptical Earth orbit in 2015. Starting approximately four days after launch, a series of five large perigee-raising maneuvers will be executed near apogee on a nearly every-other-orbit cadence. This perigee-raise operations concept requires a high-accuracy estimate of the orbital state within one orbit following the maneuver for performance evaluation and a high-accuracy orbit prediction to correctly plan and execute the next maneuver in the sequence. During early mission design, a linear covariance analysis method was used to study orbit determination and prediction accuracy for this perigee-raising campaign. This paper provides a higher fidelity Monte Carlo analysis using the operational COTS extended Kalman filter implementation that was performed to validate the linear covariance analysis estimates and to better characterize orbit determination performance for actively maneuvering spacecraft in a highly elliptical orbit. The study finds that the COTS extended Kalman filter tool converges on accurate definitive orbit solutions quickly, but prediction accuracy through orbits with very low altitude perigees is degraded by the unpredictability of atmospheric density variation.

Nomenclature

$d\rho$	=	deviation of atmospheric density
ρ	=	atmospheric density
R_E	=	Earth Radii
σ	=	standard deviation
n	=	number of Monte Carlo runs

I. Introduction

THE Goddard Space Flight Center (GSFC) Flight Dynamics Facility (FDF) will provide orbit determination and prediction support for the Magnetospheric Multiscale (MMS) mission during the mission's commissioning period prior to the checkout of the GPS-based onboard navigation system. The MMS mission will fly a formation of four identical spacecraft to study magnetic reconnection in Earth's magnetosphere. During 2015, the spacecraft will launch into a highly elliptical Earth orbit (eccentricity approximately 0.84) with a perigee altitude of 240 km, an apogee of 12 Earth radii (R_E), and an inclination of 28.5 degrees. Starting approximately four days after launch, a series of five large perigee-raising maneuvers will be executed near apogee on a nearly every-other-orbit cadence. The mission's nominal orbit, following the perigee-raising maneuvers, will range from 1.2 R_E x 12 R_E during

[1] Systems Engineer, a.i. solutions, Inc., 10001 Derekwood Lane, Suite 215, Lanham, MD 20706, AIAA Member
[2] Systems Engineer, a.i. solutions, Inc., 10001 Derekwood Lane, Suite 215, Lanham, MD 20706,
[3] Aerospace Engineer, 595.0, NASA Goddard Spaceflight Center, 8800 Greenbelt Rd, Greenbelt, MD, 20771
[4] Aerospace Engineer, 595.0, NASA Goddard Spaceflight Center, 8800 Greenbelt Rd, Greenbelt, MD, 20771

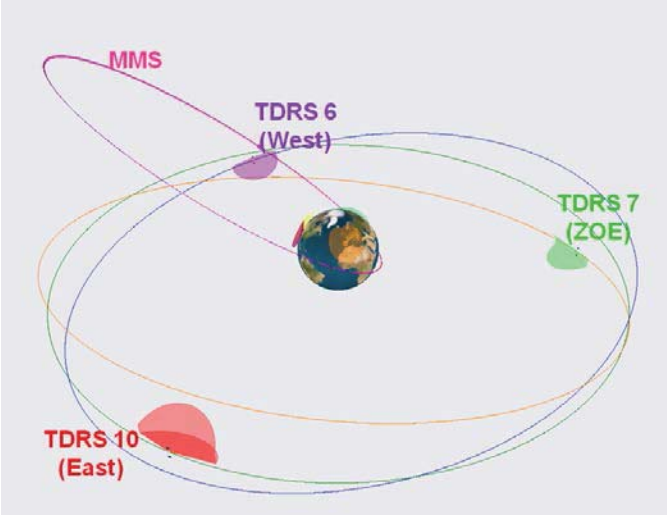

Figure 1. MMS orbits relative to TDRS orbits with tracking asset visibiltity

mission Phase 1 to 1.2 R_E x 25 R_E during mission Phase 2. Figure 1 illustrates the MMS orbit during commissioning as compared to the geosynchronous TDRS satellites.

The initial insertion orbit and early operations cadence pose a challenge to accurate orbit determination and prediction. The orbital period during this phase will be just under 24 hours driving a tight operations schedule. The low initial perigee results in high velocity transits through the Earth's atmosphere that cause significant atmospheric drag effects and uncertainty.

Throughout the mission life, a number of different orbit determination systems will be used based on system capability, readiness, and operational viability. The GSFC-developed GPS-Enhanced Onboard Navigation System (GEONS) will be used as the primary orbit determination source during the nominal mission, and radiometric-based orbit determination will only be used as a backup. However, from launch until GEONS is validated (approximately Launch + 8 weeks), the FDF will provide orbit determination using two-way Doppler tracking from the Deep Space Network (DSN) and two-way range and Doppler from the Space Network (SN) through NASA's Tracking and Data Relay Satellites (TDRS). The FDF will use a two stage orbit determination solution as follows. For early orbit determination and until the operational filter converges, the FDF will use the Goddard Trajectory Determination System[1] (GTDS) to perform orbit determination using a batch least squares method. GTDS enables fast solution generation allowing for separation state verification and acquisition data generation prior to the filter converging. It also allows for a rapid response to contingency situations. The GTDS solutions will be used to provide the *a priori* state to seed the extended Kalman filter implemented in Orbit Determination Toolkit[2] (ODTK). The extended Kalman filter is expected to require approximately one orbit to converge; once converged, the filter will provide the primary ground based solution through the end of FDF support. The FDF supported the THEMIS mission which operated in a similar orbit using only GTDS, but the THEMIS support did not levy any maneuver planning requirements on the FDF and accuracy was primarily driven by spacecraft acquisition needs.[3] The extended Kalman filter was added for its ability to solve over the sequence of perigee raise maneuvers.

The mission's flight dynamics team will plan maneuvers approximately one orbit prior to maneuver execution using the latest available definitive orbit solution and prediction. After the first maneuver, the flight dynamics team will calibrate the thrusters for planning the remaining maneuvers. The perigee raise operations concept requires a high-accuracy estimate of the orbit state within one orbit following the maneuver for performance evaluation and a high-accuracy orbit prediction to correctly plan and execute the next maneuver in the sequence. Figure 2 illustrates the operations cadence necessary through the end of the perigee raise campaign. To ensure that the maneuvers are designed appropriately, the mission imposes the following requirement on the apogee-to-apogee prediction accuracy:

> The flight dynamics design shall provide orbit solutions for maneuver planning for which the error in the velocity vector solution predicted one revolution (~24 hours) ahead to the maneuver time does not exceed 1% of the magnitude of the equivalent delta-V vector of the upcoming maneuver, or 5 mm/s RSS, whichever is greater, with probability 99%.

Prior to this analysis, the 5 mm/s threshold was expected and was given as the criteria to evaluate against for the analysis. To meet the requirement the filter must rapidly converge on an accurate solution approximately 3.5 orbits after spacecraft separation. The filter must remain converged through each of the maneuvers and, in the worst case, provide an accurate orbit state for planning the next maneuver within one orbit after the previous maneuver.

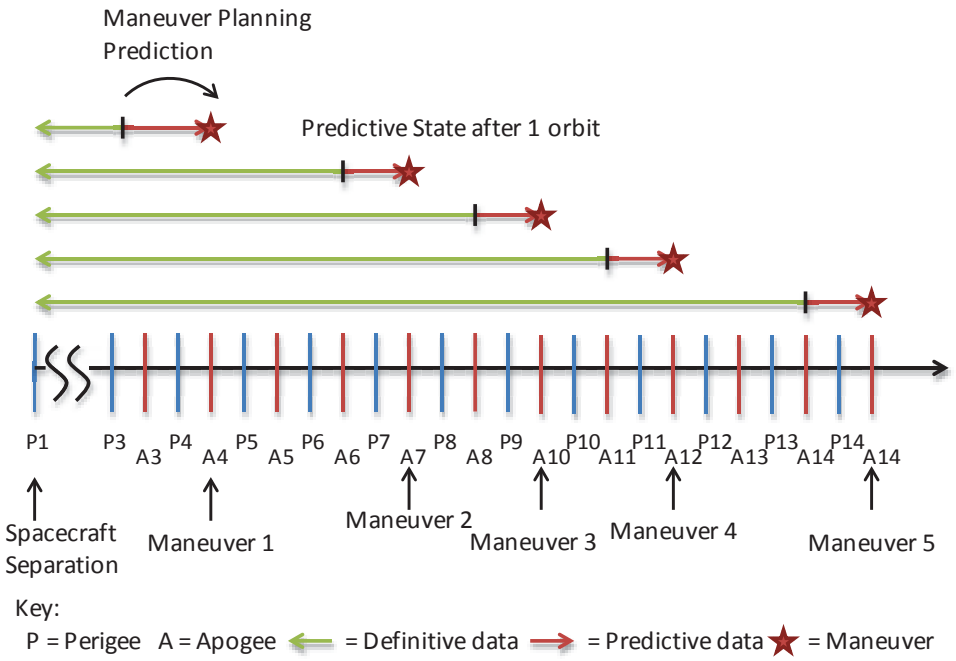

Figure 2. Illustration of maneuver prediction operations concept

The mission requires an accurate definitive post-maneuver state shortly after the first maneuver execution time in order to verify and calibrate thruster performance and plan for the upcoming maneuvers. To develop an accurate maneuver plan, the following requirement on apogee-to-apogee definitive accuracy is imposed:

> The flight dynamics design shall provide definitive orbit solutions within one revolution after the first perigee raise maneuver for which the velocity error in each component of the definitive ground orbit determination solutions at the maneuver end time does not exceed either 1% of the associated components of the equivalent delta-V vector, or 5 mm/s, whichever is greater, with probability 99%.

Figure 3 below illustrates the definitive OD requirement. To meet this requirement, the filter must rapidly re-converge or remain converged through potentially large maneuvers and provide an accurate state quickly.

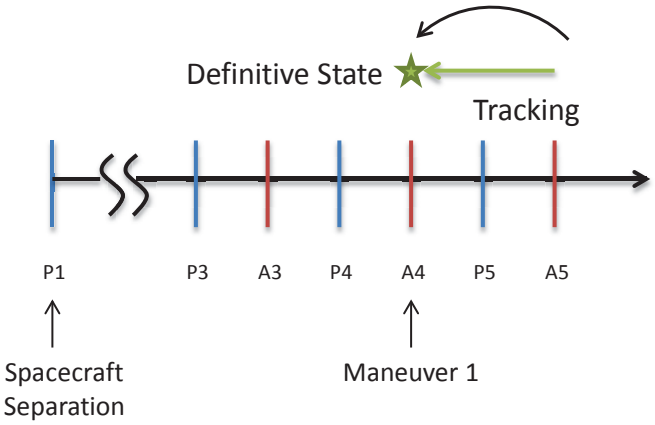

Figure 3. Definitive state comparison operations concept

During early mission design, a linear covariance analysis was used to assess the orbit determination and prediction accuracy for this perigee-raising campaign.[4] This early study looked at the expected overall accuracy during this period and the sensitivity to various factors such as tracking data type, optimal tracking data arc length (for a batch least squares solution), and tracking schedule. The analysis estimated orbit determination accuracy at a location five hours prior to the maneuver time. The study then estimated the error in the five-hour prediction to the maneuver time. The analysis also estimated the definitive post-maneuver errors using a 24- and 37-hour tracking data arc. It was found that meeting the 5 mm/s definitive and predictive threshold would be a challenge. Only one scenario using the longest OD arc and both range and Doppler data from the SN and DSN met the 5 mm/s threshold with the five-hour prediction.

This paper describes a higher fidelity Monte Carlo analysis performed to validate some of the earlier error estimates and to better characterize the orbit determination performance of the actively maneuvering spacecraft in a highly elliptical orbit. The study was performed using the tracking data simulator and extended Kalman filter orbit state estimator implemented in ODTK. The results of the analysis are presented with an investigation into the major source of prediction errors and the resulting update to the mission's predictive error requirement.

II. Analysis

This analysis uses a Monte Carlo approach to verify and characterize the definitive orbit determination and orbit prediction accuracy achievable from the Kalman filter tool that will be used operationally. The Monte Carlo approach allows variation of a wide range of orbit parameters simultaneously. The filter's performance and ability to respond to measurement and modeling errors can be characterized against the range of variation more thoroughly than other approaches.

The flow chart in Fig. 4 below outlines the basic analysis structure. The validation of the predictive and definitive requirements uses the same structure with different start and end points consistent with the operations timeline. From the externally-provided reference ephemerides, a representative tracking schedule is developed. Using the reference orbital insertion states and reference maneuver sequence, simulated truth ephemerides and associated simulated tracking data sets from the SN and DSN are generated for each of the *n* Monte Carlo samples. Each simulated observation set is processed by the extended Kalman filter tool in ODTK using perturbed *a priori* separation conditions and "mis-modeled" maneuvers. The ephemerides are post-processed and compared to the simulated truth ephemerides to generate the errors for each Monte Carlo sample. For the definitive requirement validation, a total of 100 Monte Carlo samples were created (n=100). Due to the additional processing time associated with filtering over two weeks instead of 24 hours, a total of only 75 Monte Carlo samples (n=75) were created for the predictive requirement validation.

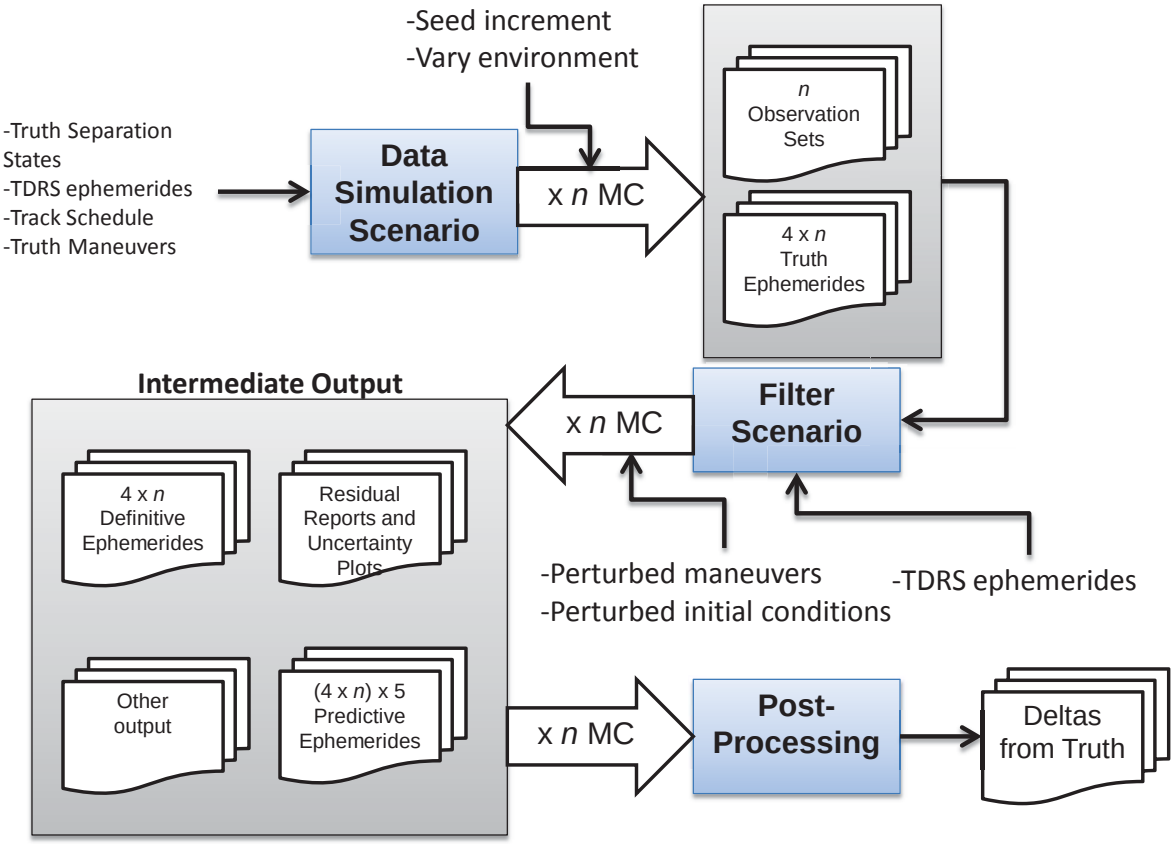

Figure 4. Monte Carlo study concept and architecture

To begin the analysis, it was necessary to develop a representative tracking schedule for the period in question. The previous linear covariance analysis study showed that range and Doppler observations from both the SN and DSN are necessary for best orbit determination performance[4]. Subsequent spacecraft design constraints dictated the use of DSN Doppler tracking and SN Doppler and range tracking. The nominal plan for tracking schedule development is to have SN tracking for four hours on either side of perigee and DSN tracking for the remainder of the orbit to allow for continuous tracking between the four spacecraft. The tracking will nominally be divided among the spacecraft in a round-robin manner with 20-minute passes separated by 10 minutes for transitioning between the spacecraft. The view periods for each of the spacecraft to each of the TDRS spacecraft and DSN stations were calculated using an early development version of the mission's ground system. Using the externally-provided reference orbit and the nominal tracking plan, a schedule of tracking passes was generated manually to ensure reasonable coverage, but it was not optimized. The TDRS and ground stations were selected primarily on ease of manual scheduling. No distinctions were made between TDRS simple, primary, or extended fields of view or specific antennas at DSN ground sites. This approach occasionally resulted in periods where all SN passes were on a single TDRS for several days and all DSN passes were at one or two ground sites. Operationally, it might be beneficial to vary the TDRS and ground site selection to reduce orbit ambiguities. Occasionally, there was no visibility to the SN or DSN. A two orbit snapshot of the schedule is illustrated by Fig. 5 below. Because the initial conditions and environmental parameters used in the simulation were perturbed to develop the simulator truth orbits, the actual visibility for each Monte Carlo case differed occasionally from the reference orbit.

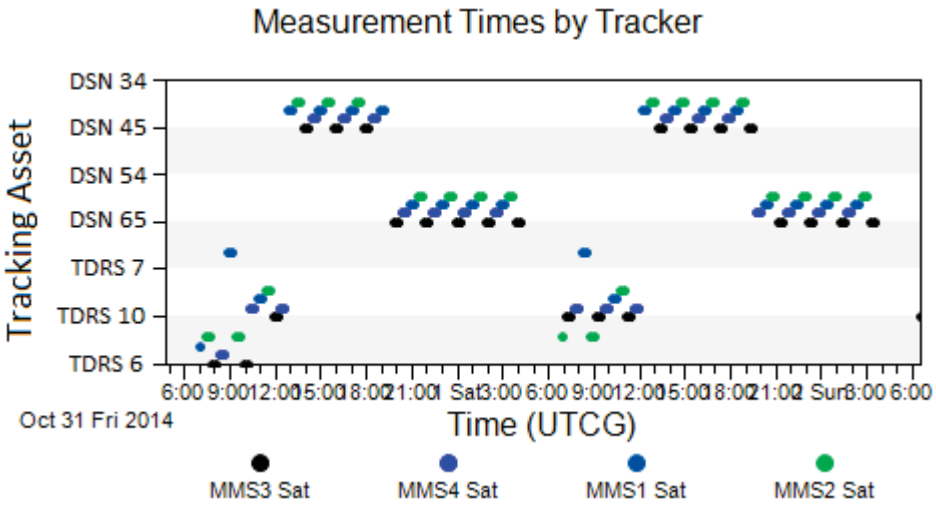

Figure 5. Satellite measurement times by tracking asset

The simulator used the reference orbital insertion states and varied orbit forces when generating the simulated truth ephemerides. For each Monte Carlo sample, the atmospheric density, ballistic coefficient, and solar radiation pressure were allowed to vary within the simulation run. Table 5 in the appendix provides the model and statistics used by the ODTK simulator to vary each of the values. The predictive requirement validation used nominal predicted solar flux values as inputs to the atmospheric density model. To be conservative, the definitive requirement validation used extreme values for the solar flux. The maneuvers were modeled within the simulator as instantaneous maneuvers of the reference magnitude and direction at the reference time. It is worth noting that because of the fixed maneuver time and varied orbit forces, the actual orbital position of the maneuver potentially differs slightly from the reference orbital position. The range and Doppler tracking data were generated using performance statistics comparable to expected SN and DSN tracking performance. Gaussian noise was added to both the range and Doppler observations, and a time varying bias was also included in the TDRS range values. The models and statistics used by the ODTK simulator to generate the observations is included in Table 6 in the appendix. Ionospheric effects were included in the simulated data. A total of 100 observation files and 400 truth ephemerides were generated by the simulator for the definitive error validation, and 75 observation files with 300 truth ephemerides were generated for the predictive error validation.

For each Monte Carlo sample, the filter was seeded with a different *a priori* orbit state that deviated from the reference state. Operationally, the FDF will generate batch least squares solutions post-separation and will feed these solutions into the filter as the *a priori* estimate of the orbit state, thus the states were deviated based on the historical

uncertainties of the FDF's early orbit batch least squares solutions. The initial Cartesian state was perturbed by a Gaussian random draw with 100 m (1-σ) uncertainty in each position component and 10 cm/s (1-σ) uncertainty in each velocity component. In the filter, maneuvers where modeled as instantaneous maneuvers. Each of the perigee raise maneuvers was mis-modeled to verify filter robustness given the expected deviations of the actual maneuvers from the planned maneuvers. An expected maneuver performance uncertainty of 2% of the total maneuver magnitude was used. The maneuver error mis-modeling was decomposed evenly into the tangential, normal, and binormal directions such that the root sum square (RSS) of the component error uncertainties was 2% of the total maneuver magnitude. The maneuvers were deviated in each direction by a random draw against a 1-σ uncertainty of $0.02/\sqrt{3}$ times the maneuver magnitude (about 1.15%). To meet definitive and predictive requirements, the filter must converge rapidly toward the truth state prior to the start of the maneuver sequence and rapidly correct for the maneuver mis-modeling after the orbit adjustment.

The filter was tuned broadly to converge over the entire Monte Carlo data set as any divergence would mean a failure of the requirements. Table 5 in the appendix presents the environment models used in the filter, and Table 6 presents the radiometric observation statistics used in the filter. The values mirrored the simulated values representing a well modeled environment and observations. The solar radiation pressure and several radiometric parameters were estimated. The atmospheric density and ballistic coefficient corrections were not estimated in the filter; instead, the nominal values were used. During the tuning phase, it was observed that estimating the atmospheric density correction and ballistic coefficient corrections in the filter reduced predictive performance. The brief transit of the atmosphere, discussed in detail later, causes poor observability of the atmospheric density and ballistic coefficient. Differencing the filter's output with the simulator output showed that the filter tended to make poor corrections; the inaccurate correction would be used in the prediction increasing the error.

The filter execution and data post-processing were separated into two processes—definitive and predictive. To validate the definitive requirement, the definitive state was investigated after the first maneuver. The filter processed the simulated observation data through one orbit after the mis-modeled maneuver. The filter output was then smoothed back through the maneuver using ODTK's smoother tool. A definitive ephemeris was generated by the smoother for the orbit following the maneuver for each of 100 Monte Carlo samples. The radial, in-track, and cross-track velocity differences between the definitive ephemeris from the smoother and the simulated truth ephemeris of the Monte Carlo sample at the maneuver time were calculated; the RSS magnitude of the velocity difference defined the sample's definitive error.

To validate the predictive requirement, the filter processed all of the tracking data up to 24 hours prior to the maneuver time (approximately one orbit) for each of 75 predictive Monte Carlo samples. The last filter state was then propagated to the maneuver time using ODTK's internal propagator. Exercising the operations concept illustrated earlier in Fig. 2, this process was conducted for each maneuver in sequence; maneuver *m*'s data arc included maneuver *m* -1. The procedure yielded 1500 predictive maneuver ephemerides. For each maneuver and each Monte Carlo sample, the velocity at the maneuver time from the predictive ephemeris was compared against the velocity from the simulator truth in a similar fashion to the definitive velocities to obtain the Monte Carlo sample's error.

The error from each Monte Carlo sample was used to compute velocity error mean, median, and maximum values for the definitive case and each of the predictive cases. The distribution of the error cannot be assumed to be Gaussian which complicates finding 99% limit. A rudimentary approach was used to determine the limit for which 99% of the results would meet the requirements. Given the number of Monte Carlo samples when subdivided by spacecraft and maneuver, a clear 99^{th} percentile cutoff could not be determined; therefore, all samples were required to be under the requirement limit. The histogram of the errors was analyzed to give a qualitative assessment of the errors. The maximum observed value was compared to the requirements to assess performance.

One concern of this method that warrants further study is the use of simulated tracking data in the Kalman filter. The simulator applies a Gaussian noise profile to the observations which is then removed by a Kalman filter that is optimized to remove Gaussian noise. Especially when using an integrated simulator and filter toolset, the concern is that the filter might remove the simulated noise much more effectively than real noise leading to better performance than would be seen operations with a real spacecraft.

III. Results and Discussion

Results from the Monte Carlo analysis suggest that the ODTK extended Kalman filter can be expected to generate highly accurate definitive solutions. In contrast, the predictive performance of the propagation from the filtered state is not accurate enough to meet the 5 mm/s error threshold for the initial very low perigee orbits. As

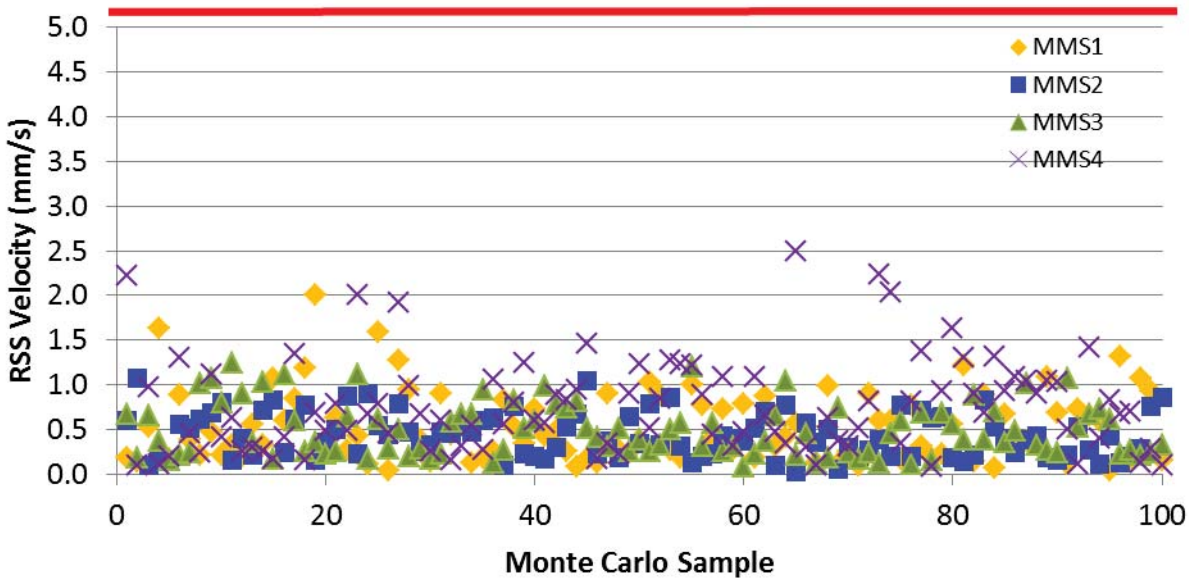

Figure 6. Definitive velocity error Monte Carlo results for first perigee raise maneuver

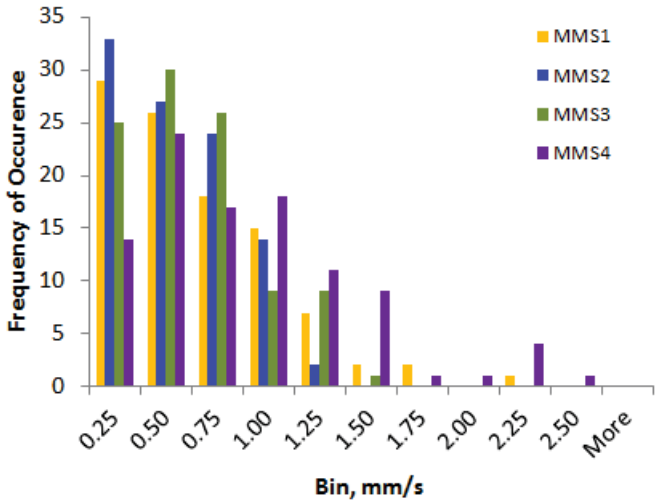

Figure 7. Histogram of definitive velocity error for first perigee raise maneuver

discussed in detail below, the predictive performance improves substantially as the perigee altitude increases and the effects of atmospheric density errors decrease.

The lower 5 mm/s threshold within the definitive requirement is met with a margin of 50% in the worst-performing Monte Carlo sample. Figure 6 presents the first perigee raise maneuver's RSS definitive velocity errors at the maneuver end time for each of the Monte Carlo samples. The upper limit on the scale is the requirement threshold. All Monte Carlo sample errors are well below even the 5 mm/s threshold. Figure 7 is the histogram of the definitive velocity error showing the error distribution.

Table 1 presents the definitive orbit determination statistics and the 1% of maneuver magnitude limit. The minimum velocity error occurs at apogee which is approximately where the error was calculated. Figure 8 illustrates the definitive velocity error over an entire orbit after the maneuver for the worst case Monte Carlo sample (MMS4 MC sample 65). The error discontinuity from the maneuver is clearly visible. In this case, the error primarily manifests in the cross-track component. In the majority of the Monte Carlo samples, the cross-track error is the largest component; this result may be due to the

Table 1. Definitive velocity error Monte Carlo error statistics

	MMS1	MMS2	MMS3	MMS4
Mean Velocity Error, mm/s	0.5	0.4	0.5	0.8
Mean Velocity Error, mm/s	0.4	0.4	0.4	0.7
Maximum Error, mm/s	2.0	1.1	1.3	2.5
1 % Maneuver Magnitude, mm/s	172.9	98.7	63.8	34.4

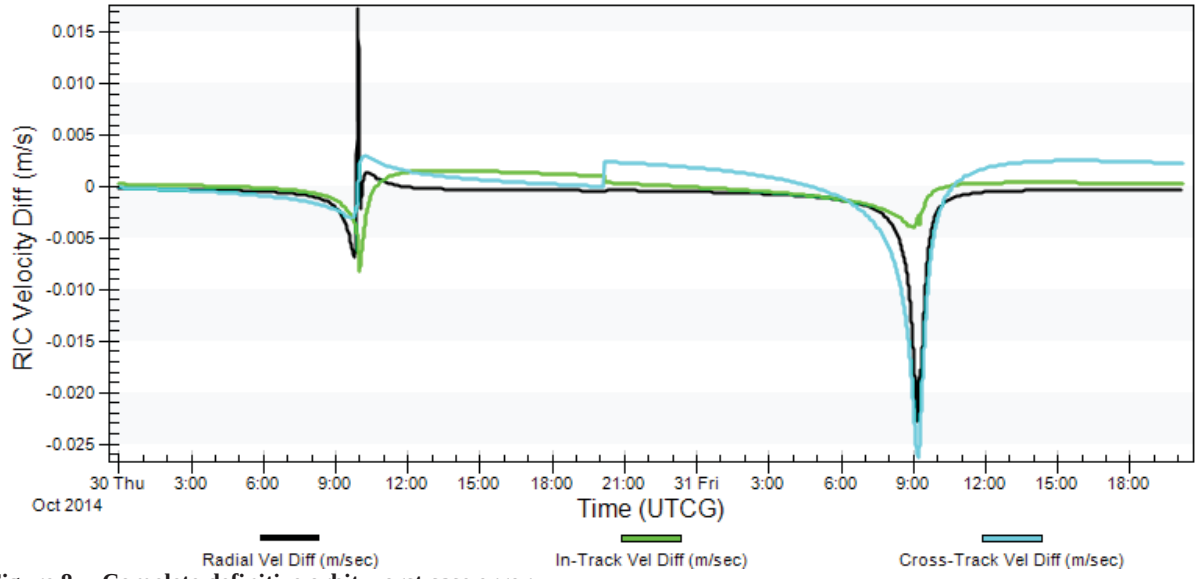

Figure 8. Complete definitive orbit worst case error

Table 2. Predictive error at maneuver time for each spacecraft and maneuver with maneuver magnitude

		MMS1	MMS2	MMS3	MMS4
Maneuver 1	Median Velocity Error, mm/s	9.18	7.83	9.09	7.29
	Mean Velocity Error, mm/s	12.61	10.23	10.20	8.74
	Maximum Velocity Error, mm/s	56.65	32.75	30.21	22.83
	1 % Maneuver Magnitude, mm/s	173.00	98.70	63.80	34.40
Maneuver 2	Median Velocity Error, mm/s	0.41	1.06	1.72	3.67
	Mean Velocity Error, mm/s	0.47	1.24	2.01	4.30
	Maximum Velocity Error, mm/s	1.39	3.65	6.63	15.91
	1 % Maneuver Magnitude, mm/s	204.30	212.40	214.80	207.00
Maneuver 3	Median Velocity Error, mm/s	0.53	0.67	0.91	0.44
	Mean Velocity Error, mm/s	0.63	1.17	1.23	0.49
	Maximum Velocity Error, mm/s	3.40	10.69	4.81	1.37
	1 % Maneuver Magnitude, mm/s	261.10	273.10	273.20	267.60
Maneuver 4	Median Velocity Error, mm/s	0.41	0.25	0.39	0.25
	Mean Velocity Error, mm/s	0.69	0.31	0.51	0.26
	Maximum Velocity Error, mm/s	6.99	0.89	3.07	0.71
	1 % Maneuver Magnitude, mm/s	127.40	134.70	133.30	133.80
Maneuver 5	Median Velocity Error, mm/s	0.16	0.17	0.19	0.19
	Mean Velocity Error, mm/s	0.20	0.17	0.20	0.22
	Maximum Velocity Error, mm/s	1.06	0.40	0.48	0.57
	1 % Maneuver Magnitude, mm/s	19.30	19.70	18.50	18.50

challenge of correctly defining the orbital plane given the single orbit of post-maneuver tracking and tracking geometry.

As shown by the statistics, the definitive error one orbit after the first maneuver is lower than the 5.3 mm/s predicted by the previous linear covariance analysis for the 37 hour data arc.[4] Within the limits of this simulation, this result might demonstrate the benefits of filtering and smoothing over the maneuver as opposed to a purely post-maneuver batch least squares approach, but linear covariance analysis is intended to provide a conservative measure of performance.

The results in this analysis follow a filter tuning effort to ensure the filter was sufficiently robust enough to converge for all cases. Operationally, the FDF expects to exploit the baseline filter

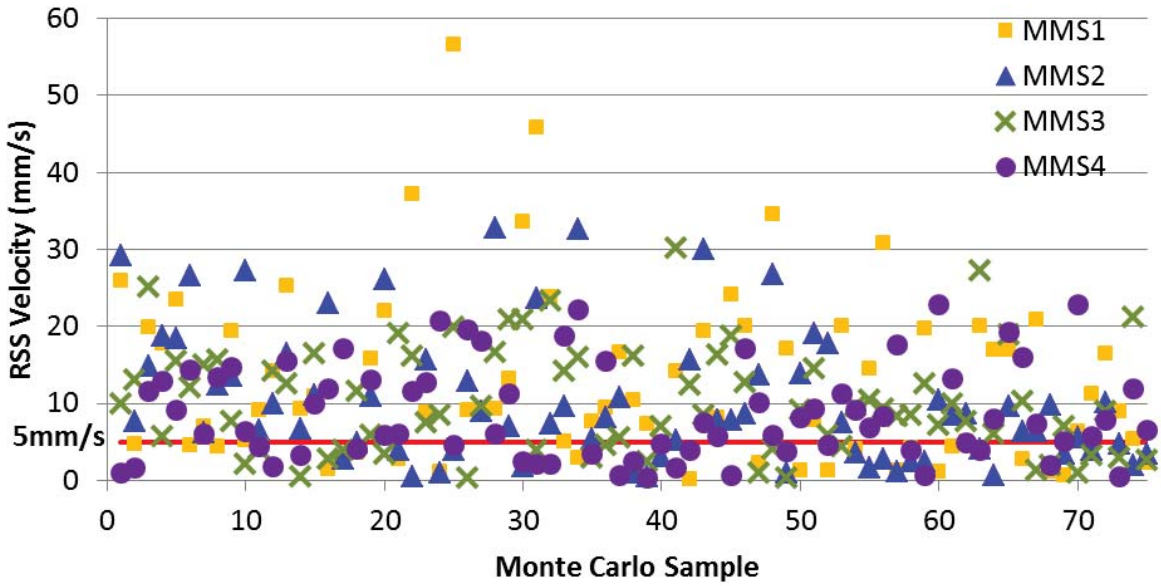

Figure 9. Monte Carlo results for predictive velocity error at apogee for first perigee raise maneuver

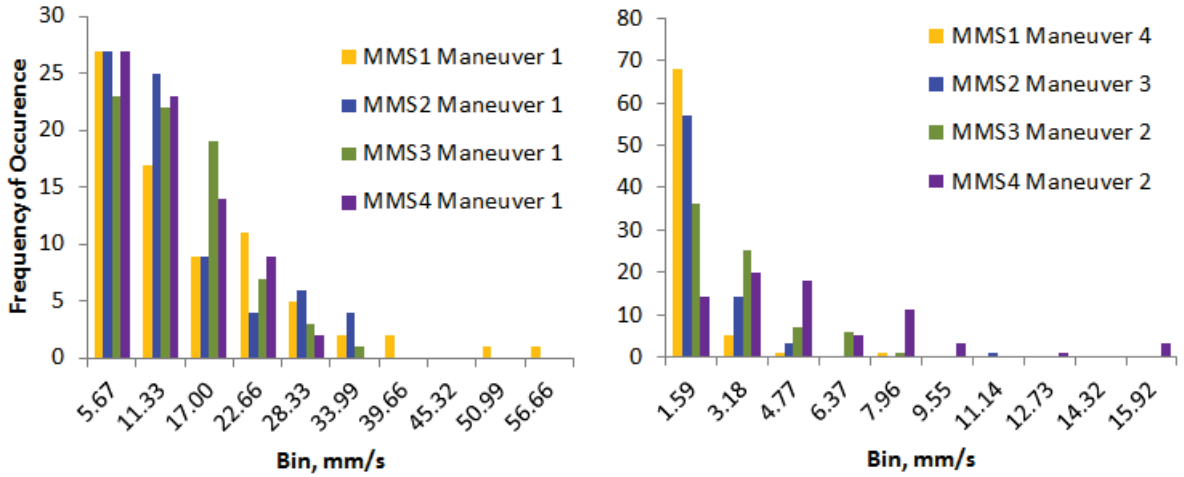

Figure 10. Histograms of definitive velocity error for perigee raise maneuvers with maximum values greater than 5 mm/s

configuration and perform near real-time tuning and re-filtering to improve the solution and correct for any possible unconverged solutions.

In contrast to the margin by which even the lower threshold within the definitive requirement was met, the predictive errors were much higher. All maneuvers met the maximum 1% of the maneuver magnitude criteria, but the 5 mm/s predictive error threshold could not be satisfied in several cases. Table 2 presents the median, mean, and maximum velocity errors with the associated maneuver magnitude for each of the maneuvers in the sequence. The highlighting indicates the maximum value failing to meet the 5 mm/s threshold. The mean and median values for the first maneuver are greater than 5 mm/s for all of the spacecraft. Each of the spacecraft have an additional maneuver with maximum values above 5 mm/s. Note that these results are from a case representing an environment and observations which are well modeled.

Figure 9 shows the spread of predictive velocity errors at the maneuver time for the first perigee raise maneuver. The figure shows how far above the 5 mm/s error threshold many of the predictions are. The maximum predictive velocity error is 56 mm/s for MMS1 (MC sample 25). The figure also illustrates the spread of the prediction errors. Figure 10 shows the histograms for all of the maneuvers with maximum values greater than 5 mm/s. On the left is the histogram for the first maneuver; on the right is the histogram for the remaining instances with maximum values

greater than 5 mm/s. The violations of 5 mm/s for MMS1 maneuver 4 and MMS2 maneuver 3 are outliers relative to the mass of the errors. For the first maneuver and MMS3 and MMS4's second maneuver, a significant portion of the errors are greater than the 5 mm/s threshold suggesting a consistent source of the errors.

The investigation into the dominant source of the predictive error for the first maneuver and MMS3 and MMS4's second maneuver points to the prediction through perigee. Figure 11 illustrates the worst case 24 hour prediction for MMS1 (MC sample 25), and Fig. 12 shows the 24 hour prediction for an example case that met the 5mm/s threshold (MC sample 24). Both of the predictions match the truth fairly well prior to perigee. The error at perigee spikes in both cases as would be expected when absolute velocity is highest. After perigee, the error in the passing case returns to a smaller absolute value as the velocity decreases, and the error slowly diverges from the truth. The worst case error diverged from the truth after perigee and continued to grow rapidly to the end of the prediction.

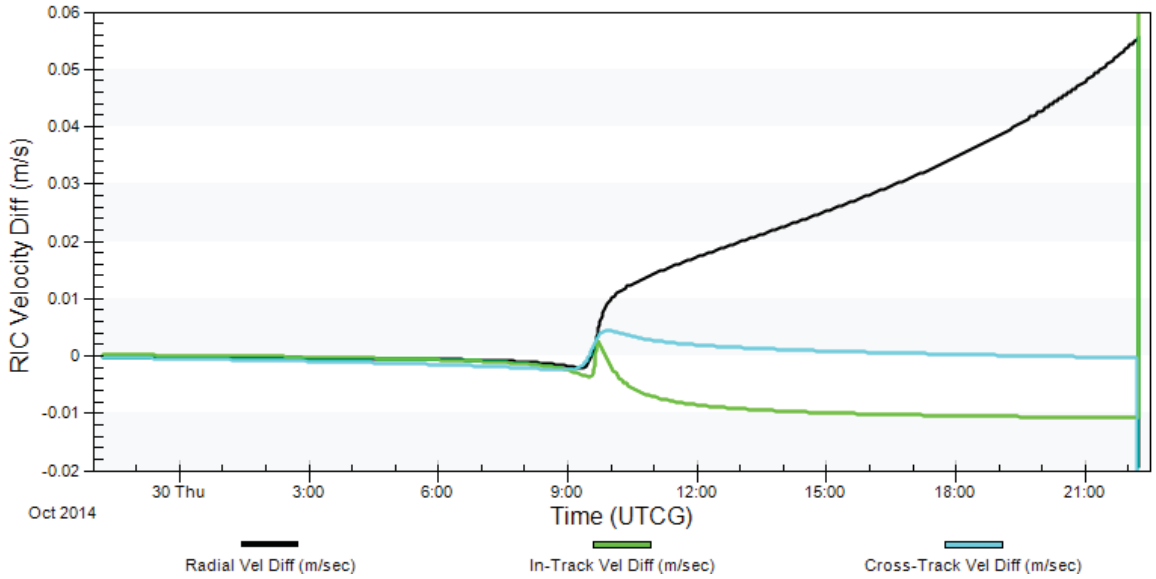

Figure 11. MMS1 maneuver 1 worst case prediction vs truth

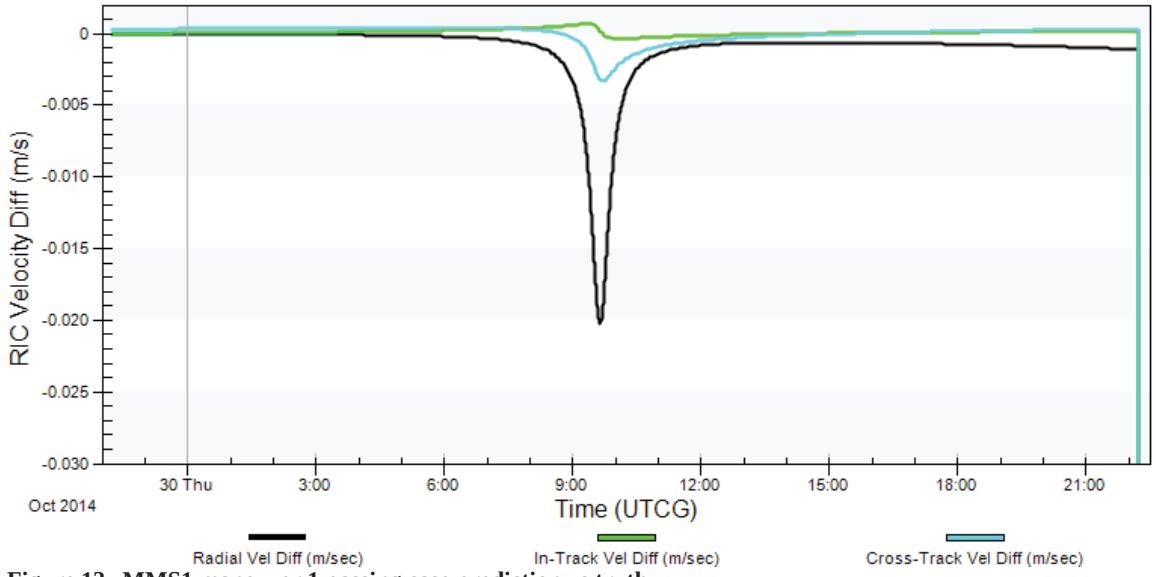

Figure 12. MMS1 maneuver 1 passing case prediction vs truth

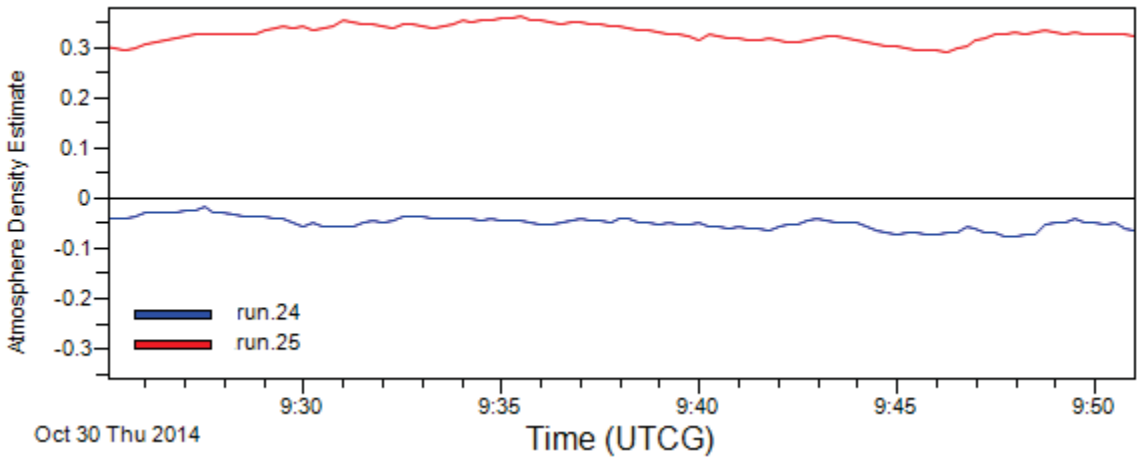

Figure 13. Simulated atmospheric density variation (dρ/ρ) near perigee for MMS1 worst case (MC sample 25) and passing (MC sample 24) prediction

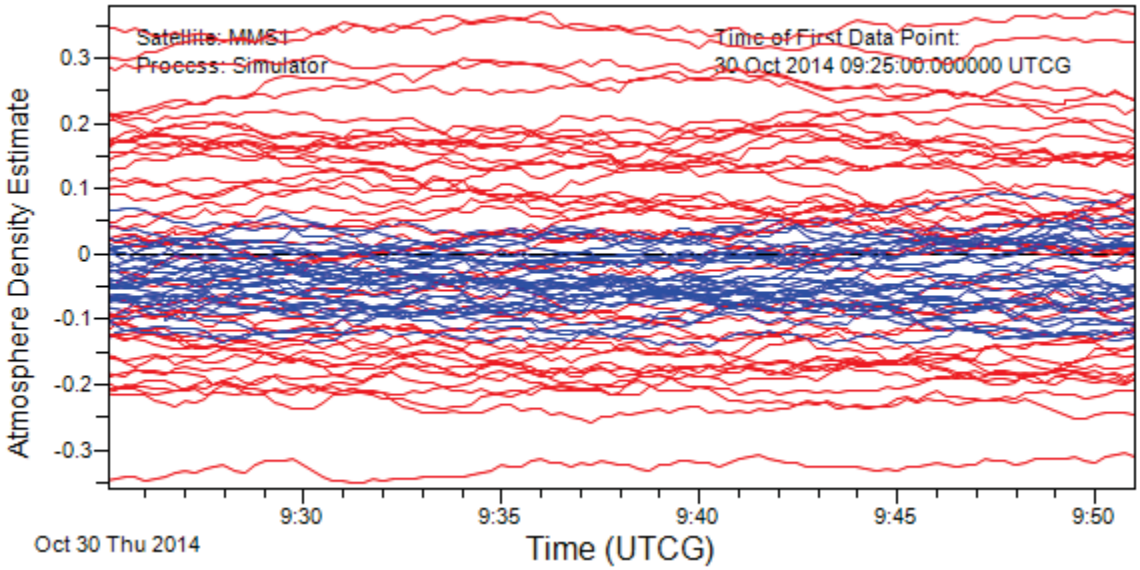

Figure 14. Simulated atmospheric density variation (dρ/ρ) near perigee for all MMS1 prediction Monte Carlo samples *(Red indicates a Monte Carlo sample with error greater than 5 mm/s. Blue indicates error less than 5 mm/s)*

The perigee error divergence is due to atmospheric density uncertainties amplified by the high velocity of the spacecraft. The nominal insertion orbit for the MMS mission has a perigee altitude of approximately 240 km and an apogee of about 12 R_E which yields a velocity at perigee of approximately 10.5 km/s. Given this initial orbit, there are only about 8 minutes on either side of perigee during which the spacecraft are below 1000 km. In both the simulator and filter, 1000 km is the cutoff above which atmospheric effects are not applied. Figure 13 shows the simulated atmospheric density variation that occurs when the spacecraft is near perigee for the worst case prediction and for the passing prediction corresponding to Figs. 11 and 12. The atmospheric density variation is shown as the deviation of the density, dρ, over the nominal density, ρ. The perigee time for MMS1 is approximately 9:38 UTCG, thus the atmosphere transit is between 9:30 UTCG and 9:46 UTCG. During the transit window for the worst case, the atmospheric density is much higher than the nominal value. In contrast, the atmospheric density for the passing case has a smaller absolute variation and the sign indicates a lower density than the nominal value. Figure 14 shows the simulated atmospheric density variation for all Monte Carlo samples during MMS1's first maneuver where blue indicates the Monte Carlo sample meets the 5mm/s predictive threshold and red indicates a failure to meet the threshold. All of the passing Monte Carlo samples had small absolute variation and skewed towards a lower density than the nominal value. When predicting through perigee, the nominal uncorrected atmospheric density or an

estimated correction from the previous orbit almost 24 hours prior must be used. Accurate atmospheric density modeling and prediction is a significant challenge even for low Earth orbiters with large data volumes and significantly higher perigee altitudes than the initial MMS perigees.[5,6] Given the variation in atmospheric density over a day, having an accurate atmospheric density correction for the brief atmosphere transit of MMS would be difficult. The perturbation force due to atmospheric drag grows linearly with the density and with the square of the velocity.[7] At the MMS spacecraft's initial low perigee altitude, the perturbation force can be significant and not readily predictable. When the orbit is propagated through the low perigee altitude, the error as compared to truth can be significant as seen in this analysis.

Table 4. Nominal perigee altitudes after each maneuver

	MMS1	MMS2	MMS3	MMS4
Separation, km	240	244	242	241
Post-Maneuver 1, km	520	410	355	310
Post-Maneuver 2, km	830	440	680	610
Post-Maneuver 3, km	1230	1170	1120	1120
Post-Maneuver 4, km	1430	1400	1340	1230
Post-Maneuver 5, km	1480	1460	1390	1280

As the force of the atmospheric drag perturbation decreases as the perigee altitude increases, the prediction accuracy improves substantially. After the second maneuver all of the spacecraft had perigee altitudes high enough that the filter was generally capable of accurately predicting through perigee. MMS3 and MMS4 both failed to meet the 5 mm/s predictive threshold for a significant portion of the samples after the first maneuver due to the smaller magnitudes of their first maneuvers. Table 3 presents the nominal perigee altitudes after each of the maneuvers. This effect was not observed during FDF's THEMIS support as the initial perigee altitudes where greater than 400 km.[3]

Table 3. Definitive and predictive position errors at apogee

	MMS1	MMS2	MMS3	MMS4
	Maneuver 1 Definitive			
Median Error, m	20.5	18.2	17.0	17.9
Maximum Error, m	74.9	51.7	56.0	50.9
	Maneuver 1 Predictive			
Median Error, m	217.6	191.6	197.2	154.8
Maximum Error, m	1316.9	749.4	671.0	488.3
	Maneuver 2 Predictive			
Median Error, m	12.0	26.6	36.7	75.4
Maximum Error, m	41.8	83.7	142.5	344.7
	Maneuver 3 Predictive			
Median Error, m	8.3	11.4	10.1	10.1
Maximum Error, m	23.6	82.3	32.6	31.4
	Maneuver 4 Predictive			
Median Error, m	6.8	9.2	6.2	5.8
Maximum Error, m	23.8	98.0	23.5	16.8
	Maneuver 5 Predictive			
Median Error, m	5.4	6.1	5.5	5.9
Maximum Error, m	18.3	60.4	17.5	14.7

Finally, there is not a position error requirement that must be met during FDF support. For completeness, Table 4 presents the median and maximum values for the definitive and predictive position errors at apogee. The position errors behaved in a similar manner to the velocity errors. The definitive error after the first maneuver is low. The predictive position error was large for the low perigee prediction cases.

IV. Conclusion

A Monte Carlo analysis to evaluate orbit determination and prediction requirements during the MMS commissioning orbit is detailed. The analysis found that the mission's desired predictive accuracy limit of 5mm/s velocity error could not be met due to atmospheric density variation. This is not an unexpected result, as the previous linear covariance analysis found that it would be a challenge to meet the 5 mm/s predictive threshold using a five hour prediction that did not pass through perigee. As a result of the analysis presented here, the 1% of maneuver magnitude scaling was added to the predictive accuracy requirement. The scaling of the predictive

requirement ensures that the predictive error is of the same order of magnitude as the expected maneuver burn uncertainties of 1-2%.

The results of the definitive analysis are unexpected. The error was much lower than was predicted by the previous linear covariance analysis study. This result demonstrates the benefits of using a Kalman filter over maneuvers as opposed a purely batch least squares orbit determination methodology. If these results are ultimately validated by operational results, it will also demonstrate the necessity, in some cases, of using the Monte Carlo approach for OD accuracy estimation as opposed to an overly conservative linear covariance analysis approach.

Appendix

Table 5 Force and Environment models and associated data

Atmospheric Density Correction	Simulated		Not Estimated
	Atmospheric Density Model*		Jacchia-Roberts
	Half-life		3 hrs
	Solar Flux†	Predictive	Definitive
	F10	100	145
	F10bar	100	145
	Ap	10	9.985
Ballistic Coefficient Correction	Simulated		Not Estimated
	Ballistic Coefficient Model		GaussMarkov
	CD		2.2
	Area		7.1 m^2
	Initial Estimate		0
	Sigma		0.05/0.1‡
	Half-life		480 hrs
Solar Pressure	Simulated		Estimated
	Model		Spherical
	Area		2.02671 m^2
	Constant		1.8
	Sigma		0.3
	Half-life		480 hrs
Gravity Model	EGM96		
	Degree and Order		21
Propagator	RKF 7(8)		
	Relative Error Tolerance		$1x10^{-13}$
	Minimum Step Size		1 s

* Model parameters detailed in reference 7, but it is worth noting the sigma is a function of altitude starting from ~0.02 at 110km and peaking at 0.4 near 600 km.

† Used static solar flux inputs from January 2013 Schatten predictions[8] for October 2014 in the predictive case. Used extreme values for the definitive case.

‡ Used 0.05 for the predictive case and 0.1 for the definitive case.

Table 6 Measurement models and associated data

Satellite to Ground Transponder Bias	Not Simulated	Not Estimated
Satellite to TDRS Transponder	Simulated	Estimated
	Model	GaussMarkov
	Constant	0
	Sigma	29.9792 m
	Half-life	480 hrs
TDRS Relay Bias	Simulated	Estimated
	Model	GaussMarkov
	Constant	272.511 m
	Sigma	1.49896 m
	Half-life	2400 hrs
TDRS Range Statistics	Simulated	Estimated
	Bias Model	GaussMarkov
	Bias Constant	0 m
	Bias Sigma	7 m
	Bias Half-life	1 hrs
	White Noise Sigma	1.5 m
TDRS Doppler Statistics		
Bias	Not Simulated	Not Estimated
	White Noise Sigma	0.01974 Hz
DSN Doppler Statistics		
Bias	Not Simulated	Not Estimated
	White Noise Sigma	0.1 cm/s

References

[1]ODTK, Orbit Determination Tool Kit, Software Package, Ver. 6.1.3, Analytical Graphics, Inc, Greenbelt, MD, 2014.

[2]GTDS, Goddard Trajectory Determination System, Software Package, Ver, 2012 v1.0, NASA Goddard Spaceflight Center, Greenbelt, MD. 2014.

3Morinelli, P., Cosgrove, J., Blizzard, M., Nicholson, A., and Robertson, M., "Orbit Determination and Navigation of the Time History of Events and Macroscale Interactions during Substorms (THEMIS)," *20th International Symposium on Space Flight Dynamics*, Annapolis, MD, 2007, URL: http://issfd.org/ISSFD_2007/20-5.pdf [cited 6/1/14]

[4]Chung, L. R., Novak, S., Long, A., Gramling, C., "Magnetospheric Multiscale (MMS) Mission Commissioning Phase Orbit Determination Error Analysis", *Advances in the Astronautical Sciences 135, no. 1, 200, p 355-374.*

[5]Vavrina, M. A., "Improving Fermi Orbit Determination and Prediction in an Uncertain Atmospheric Drag Environment," *24th International Symposium on Space Flight Dynamics, Laurel, MD, 2014,* URL: https://dnnpro.outer.jhuapl.edu/Portals/35/ISSFD24_Paper_Release/ISSFD24_Paper_S8-5_Vavrina.pdf [cited 6/1/14]

[6]Vallado, D. A., Finkleman, D., "A Critical Assessment of Satellite Drag and Atmospheric Density Modeling," *AIAA/AAS Astrodynamics Specialist Conference and Exhibit,* AIAA, Washington, DC, 2008, pp. 18-21

[7]Wright, J.R., "Orbit Determination Tool Kit Theory & Algorithms", Analytical Graphics, Inc., 2013, URL: https://www.agi.com/downloads/resources/white-papers/ODTK-Theory-and-Algorithms.pdf [cited 6/10/14]

[8]Schatten, K. "Fair space weather for solar cycle 24." *Geophysical Research Letters*, Vol. 32, No. 21, 2005